Steel and Composite Structures, *Vol. 29, No. 3 (2018) 391-404*
DOI: https://doi.org/10.12989/scs.2018.29.3.391

Evaluation the behavior of pre-fabricated moment connection with a new geometry of pyramidal end block under monotonic and cyclic loadings

Seyed Morteza Kazemi [1a], Mohammad Reza Sohrabi [*1] and Hasan Haji Kazemi [2b]

[1] *Civil Engineering Department, University of Sistan and Baluchestan, Zahedan, Iran*
[2] *Civil Engineering Department, Ferdowsi University, Mashhad, Iran*

(*Received October 29, 2017, Revised April 13, 2018, Accepted July 7, 2018*)

Abstract. Researchers have been long studying new building implementation methods to improve the quality of construction, reduce the time of assembly, and increase productivity. One of these methods is the use of modular pre-fabricated structural forms that are composed of a beam, column, short column, pyramidal end block, and connection plates. In this study, a new geometry for the pyramidal end block was proposed that helps facilitate the assembly procedure. Since the proposed configuration affects the performance of this form of connection, its behavior was evaluated using finite element method. For this purpose, the connection was modeled in ABAQUS and then validated by comparing the outputs with experimental results. The research proceeded through analyzing 16 specimens under monotonic and cyclic loading. The results indicated that using the pyramidal end block not only makes the assembly process easier but also reduces the out-of-plane displacement of the short column webs and the vertical displacement of beam end. By choosing appropriate section properties for column and beam, the connection can bear a rotation up to 0.01 radians within its inelastic region and a total of 0.04 radians without any significant reduction in its bearing capacity.

Keywords: cyclic loading; finite element method; modular pre-fabricated structural form; monotonic loading; pyramidal end block

1. Introduction

For decades, population growth has accelerated the speed of construction industry in every parts of the word. Today, housing is considered to be one of the most important problems. Given that traditional construction methods are not useful and efficient, the use of modern materials and techniques in this industry is essential. Compared to traditional methods, modular pre-fabricated structural forms offer several benefits that reduce costs, speed up the construction and implementation process and enhance the quality of production. All these advantages make this structural form a good solution for the problems.

The main focus of this research is to investigate the behavior of a newly proposed modular pre-fabricated structural form. In this form, the entire manufacturing process for columns, beams, doors, windows and roofs is done in factory and then the components are carried and bolted in the field. This structural form is composed of tubular columns with rectangular cross-section having horizontal connection plates at each end. The beams are made up trusses that include two angle sections as the top and bottom flange which are connected with diagonal angle sections. In order to connect the interstory columns, a short column is provided with a tubular cross-section and connection plates at each end. These connection plates are welded to the short column and then bolted to the column connection plates. The beam is then welded to the connection plates or bolted with cover plates. Fig. 1 shows the components of the connection and the way the beam is connected to the plates. To facilitate the assembly procedure and improve the bearing capacity of the connection, a pyramidal end block has been proposed but whether it affects the behavior of this type of structural form requires further investigations. All components of this structural form are fabricated in factory and in large quantities. According to Liu *et al*. (2015), these components can be easily installed and offer lower construction costs and time.

Among different structural elements, connections are the most important components in any constructional forms. After the 1994 Northridge earthquake (Miller 1998), it was found that the cause of many major building damages was due to connection failure. In this study, a proposed geometry for pyramidal end block is presented and the effect of using this additional part as well as the change of column, beam and short column section properties on the connection behavior is evaluated in terms of different amounts of plastic section modulus.

2. Review of the literature

The modular pre-fabricated structural form has attracted a lot of attention from many researchers. Sabbagh *et al*.

*Corresponding author, Associate Professor, E-mail: sohrabi@hamoon.usb.ac.ir
[a] Ph.D. Student, E-mail: kazemi.mkt@pgs.usb.ac.ir
[b] Professor, E-mail: hkazemi@um.ac.ir

Copyright © 2018 Techno-Press, Ltd.
http://www.techno-press.org/?journal=scs&subpage=6
ISSN: 1229-9367 (Print), 1598-6233 (Online)

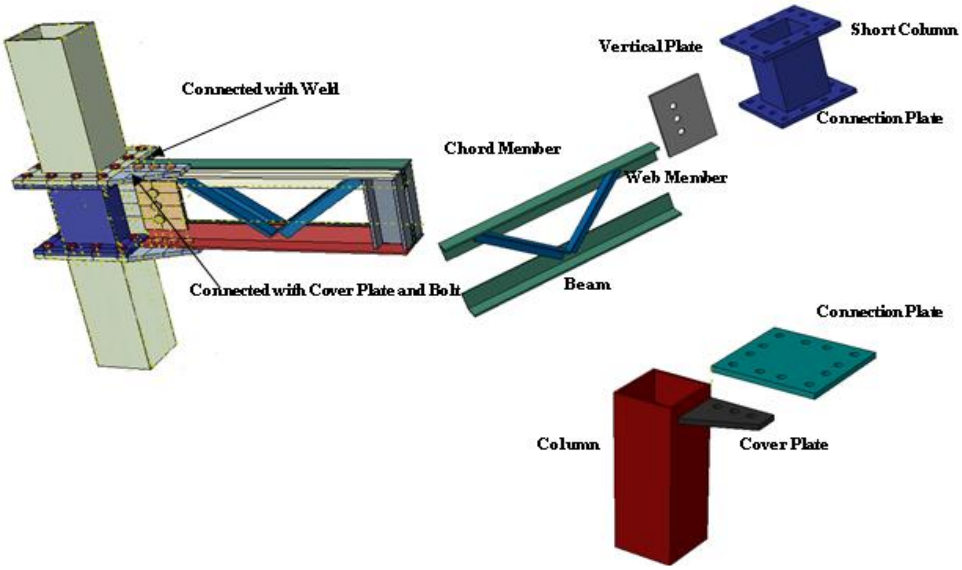

Fig. 1 Components of connection

(2013) studied the behavior of cold rolled steel frames with bolt rigid connections under cyclic loads. Maggi *et al*. (2005) used ANSYS for the numerical simulation of this structural form and compared the FEM results with experimental results under monotonic loading. Gerami *et al*. (2010) studied the effect of bolts arrangement in steel connections endplates and T- stub under cyclic loading using ABAQUS. They modeled 14 specimens of this type of connection by changing the horizontal and vertical arrangement of bolts.

The results indicated that the moment capacity and the initial rotational stiffness of T-stub bolted connections are higher than the endplate bolted connections designed based on AISC as the total energy dissipation of both groups to be approximately equal. Costa-Neves *et al*. (2013) evaluated the effect of perforated shear connectors on composite girders under monotonic loading. They studied several variables including shear connector geometry as well as the provision of transverse reinforcement within a shear connector holes. Using ABAQUS, Alhendi and Celikag (2015) attempted to improve the moment-rotation curve of reverse channel connections by changing geometrical shape. The results showed that all of the species at least have a rotation capacities up to 0.03 radians. Most of the species have a rotation capacities up to 0.06 radians while the capacity of one of them reached to 1.6 radians. Kulkarni and Gaurang (2014) studied the reduced beam connections made of Indian section under cyclic loading. The findings suggested that the connections have a good capacity under cyclic load. Ismail *et al*. (2016) studied the behavior of bolted end-plate steel connections. Using ABAQUS for modeling, they evaluated the initial stiffness, resistance and rotation capacity for these connections. Zahmatkesh *et al*. (2016) evaluated the structural performance of steel beams with slant end-plate connections. They proposed a simple method for evaluating the behavior of these beams with various dimensions under different temperatures. Herrera *et al*. (2013) tested 22 built-up T-stub connections under monotonic tensile loading. In their work, fillet welds were used to fabricate the specimens. They observed no signs of weld damage. Most specimens failed by fracture of the tension bolts after the deformation of the T flange caused by bending. Ataollahi *et al*. (2016) evaluated a new RBS connection under cyclic loading. The behavior of extended end-plate connections with European steel profiles was also assessed under this type of loading by Akgőnen *et al*. (2015).

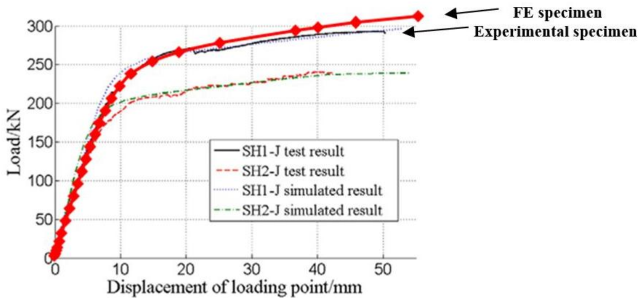

Fig. 2 Force-displacement curves for experimental and FE specimens

3. Finite element analysis

To verify the modeling procedure, the specimen of Liu *et al*. (2015) was modeled using ABAQUS. For all of the components, Q235B steel, S10.9 bolts, and standard holes were used. Pre-tension force was applied to the all of the bolts according to their types and sizes (Salmon *et al*. 2009). In order to configure the tangential behavior, the Penalty friction formulation was used with the friction coefficient of 0.303 between the bolts and the connection plates, which was the average value of three friction test models that were 0.29, 0.30 and 0.32 (JGJ82 2011). dimensions of the connection components were selected according to the experimental specimen of Liu *et al*. (2015). Force-displacement curves of experimental specimen and

FE model are shown in Fig. 2. The yielding force (Py) of SH1-J and FE model are 162.99 kN and 164.6 kN respectively, which differ only one percent and shows an acceptable agreement to validate the finite-element model. In order to assess the sensitivity of the results to the mesh density, various analyses were performed with different mesh sizes. It was found that using a mesh size equal to the half of the angle flange thickness for the high-stress parts yields proper results in the view of time and accuracy. The mesh becomes lighter on low-stress parts to reduce the time of analysis. For all of the specimens, the simulation was proceed using 3D solid element C3D8R and structural meshing technique.

4. The proposed geometry for pyramidal end block

In this form, ceilings can be constructed completely in factory, then carried to the site and placed on the column. The implementation of the pre-fabricated ceilings is difficult, practically on the upper floors. In this paper, a new method was proposed to facilitate the assembly procedure. To this aim, a pyramidal end block was added on the connection plate of columns in a way that during the ceilings implementation, the pyramidal end block is placed into the short column. Fig. 3 indicates the implementation process using the pyramidal end block. In addition to facilitate the assembly, this pyramidal end block can also affect the performance of the connection. To do so, a proper dimension was herein proposed for the pyramidal end block. The width of the rectangular part of this section is selected to be 4 mm less than the inner-part of the short column. By selecting a larger width, the section may not affect the connection performance while by using a smaller width, implementation procedure becomes difficult. Additionally, regarding the fact that standard hole sizes are used for bolts, the proposed dimension can be still effective. The inner angle of the pyramidal section was selected to be 45 degrees and its height was 30 mm less than the height of the short column. Fig. 4 shows the dimension of the pyramidal end block which can be constructed and implemented through the following steps that are indicated in Fig. 5.

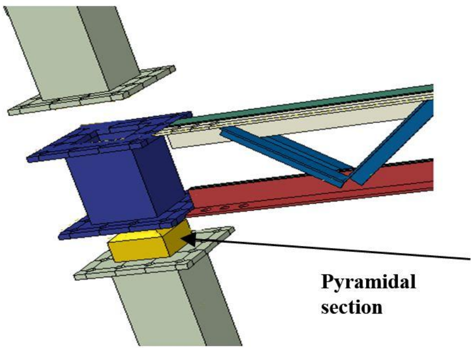

Fig. 3 Implementation process with this pyramidal end block

5. Evaluating the performance of connection

In this section, the performance of connections under

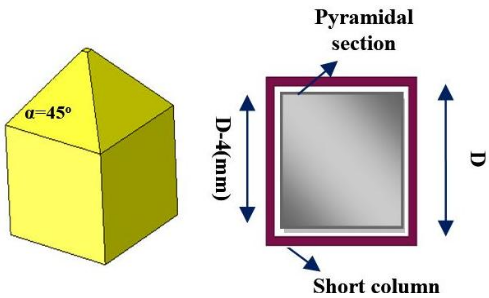

Fig. 4 Dimensions of the pyramidal end block

Construction proces of pyramidal end block

Construction process of short column

Fig. 5 Construction process of connection components in laboratory

monotonic and cyclic loading was evaluated under two conditions that were all of the connection components except short column were designed to be rigid, and in addition to the short column, beam, column and vertical plates were also ductile. In the following, loading protocol, material properties and dimensions of the connection components were described.

5.1 loading

The entire specimens went under monotonic and cyclic loading. In order to apply monotonic loading, a point load was assigned at the end of the beam and the load was applied with an amplitude began from zero and increased to a certain amount with increments of 1 kN. In cyclic loading, loads are applied through controlling displacement at the end of beam according to SAC2000 loading protocol (FEMA 2000) which are shown in Table 1 and Fig. 6.

5.2 Material and model

St37 steel was used for all specimens with elastic modulus of 2.1e^6 kg/cm^2. The material properties used in FE modeling are presented in Fig. 7. The frame, modeled in this study, is a part of the construction frame that was chosen according to SAC2000. The dimension of the components and frames are presented in Fig. 8 and Table 3.

5.3 Properties of frame and sections used in modeling

In order to obtain comparable results, the model was analyzed gradually and carefully from one component to the next. To do so, all of the components except the short column were firstly assumed to be rigid and then the connection behavior was evaluated with different thicknesses for the short column plates with and without pyramidal end block. This was continued by changing the element type of the remaining components from discrete rigid to deformable type. The reason behind going through this process was to evaluate the effect of each component on the behavior of the connection. In addition, the bolts were not modeled and the connection plates were connected together using “tie” constraint. The name and properties of specimens are presented in Table 3.

Fig. 9 indicates the force-displacement curve for specimens having the short column with different thick-

Table 1 Cyclic loading according to SAC protocol

Step	Peak deformation θ (rad.)	Number of cycles	Beam end displacement (mm)
1	0.00375	6	±9.1875
2	0.005	6	±12.25
3	0.075	4	±18.375
4	0.01	2	±24.5
5	0.015	2	±36.75
6	0.02	2	±49
7	0.03	2	±73.5

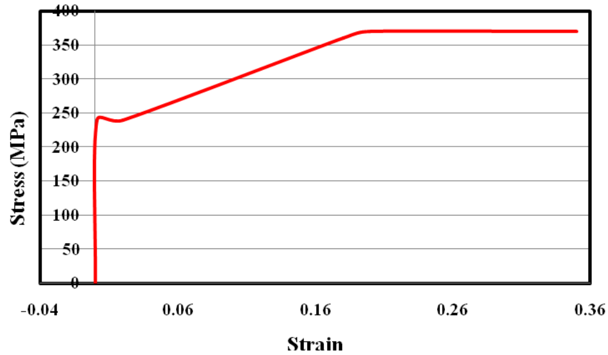

Fig. 7 Stress-strain curve of ST37 (Gerami *et al*. 2010)

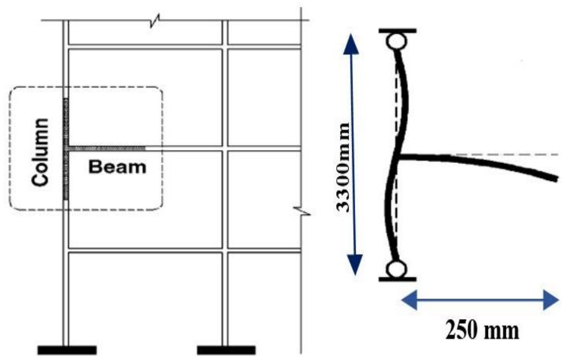

Fig. 8 The lengths of components in FE modeling

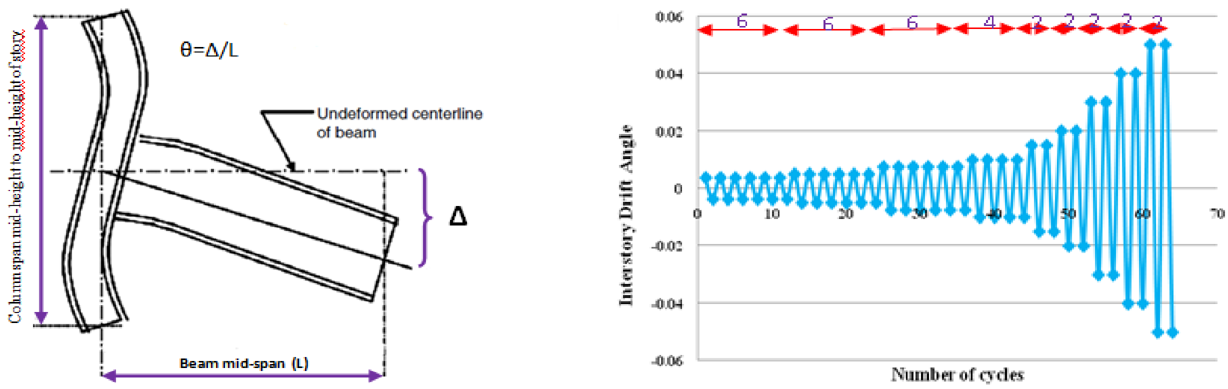

Fig. 6 FEMA/SAC2000 loading protocol in accordance with FEMA350 (FEMA-350, 2000).

Table 2 Size and dimension of connection components

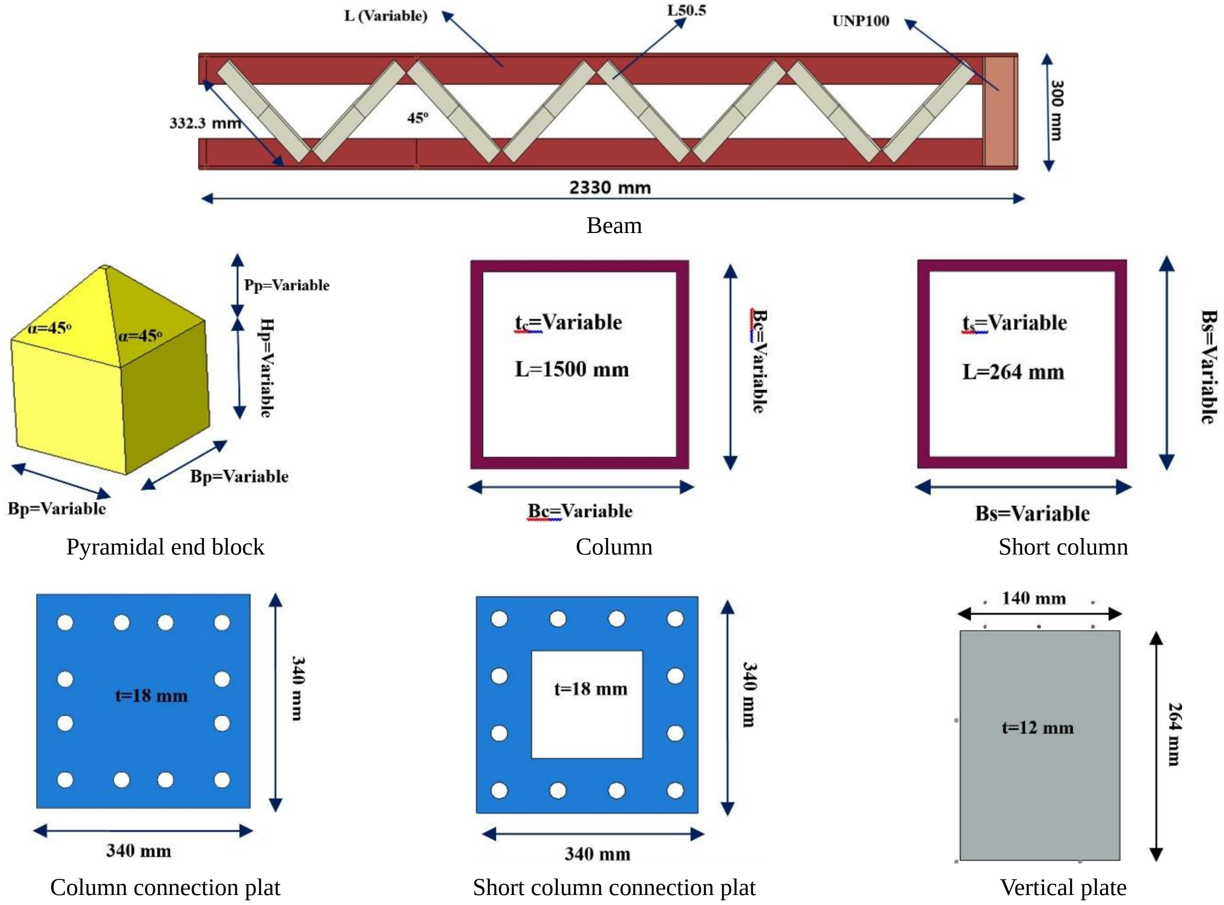

Table 3 Summary of numerical specimen details

Specimen	ts (mm)	Bs (mm)	Bp (mm)	Hp (mm)	Pp (mm)	Column, Beam, Connection plates
CBt10	10	200	-	-	-	rigid
CBt12	12	200	-	-	-	rigid
CBt15	15	200	-	-	-	rigid
CBt18	18	200	-	-	-	rigid
CBt10P	10	200	176	146	88	rigid
CBt12P	12	200	172	148	86	rigid
CBt15P	15	200	166	151	83	rigid
CBt18P	18	200	160	154	80	rigid

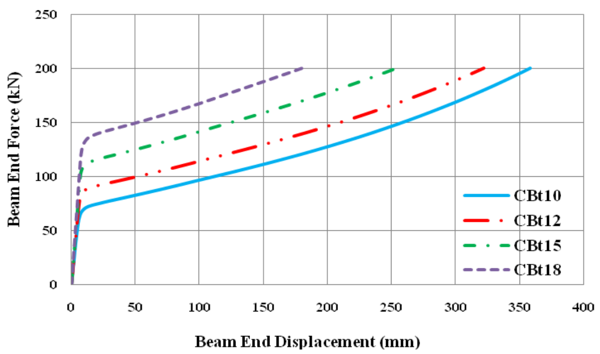

Fig. 9 Force - displacement curves for specimens without pyramidal end block

nesses and without pyramidal end block. Figs. 9 to 13 also show the effect of adding pyramidal end block on the force-displacement curve. The maximum force applied at the end of the beam in these specimens was 200 kN. For all of the specimens, Py which represents the amount of force when a part of components of the connection yields, D_y which is the amount of displacement at the end of the beam when a part of components of the connections yields and D_{200} which represents the amount of beam end displacement when force reaches to 200 kN were presented and compared to CBt10 in Table 4. This table also includes the changes caused by using pyramidal end block. It can be noted that that increasing the thicknesses of short column plates increases the stiffness of connection as well as P_y and D_y

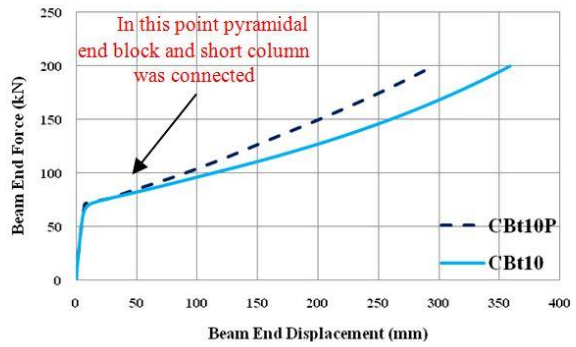

Fig. 10 Force - displacement curves for CBt10 and CBt10P

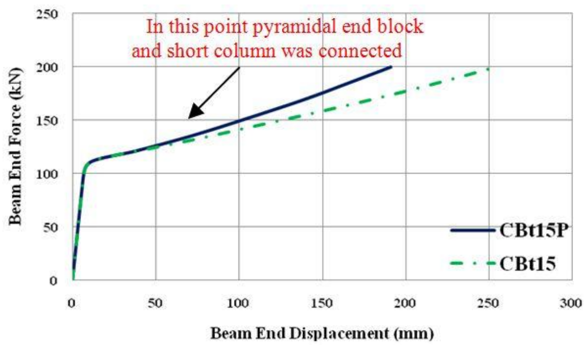

Fig. 12 Force - displacement curves for CBt15 and CBt15P

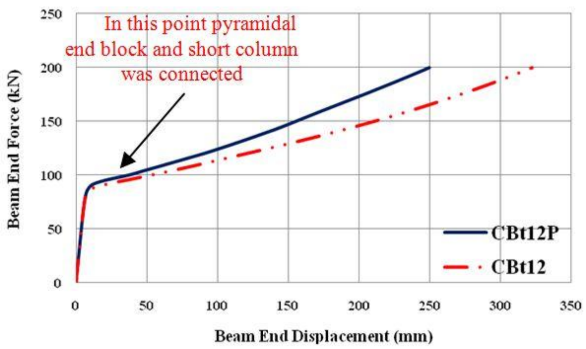

Fig. 11 Force - displacement curves for CBt12 and CBt12P

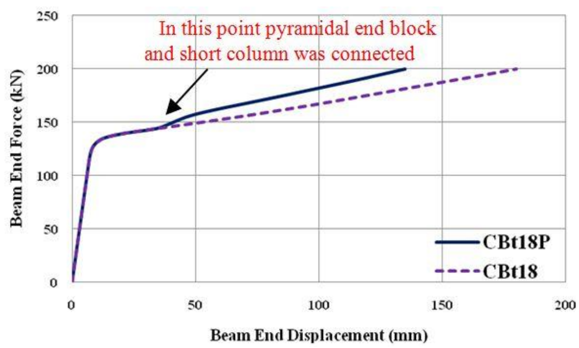

Fig. 13 Force - displacement curves for CBt18 and CBt18P

while decreases D_{200}. Based on this, a 20 percent increase in thicknesses of the short column plates increased P_y and D_y up to 26.6 and 7.12 percent and decreased D_{200} by 10.06 percent. In a similar proceeding, a 50 percent increase in thicknesses of short column plates increased P_y and D_y by 66.7 and 20.64 percent and decreased D_{200} down to 29.05 percent. Similarly, an 80 percent increase in thicknesses of short column plates increased P_y and D_y by 93.3 and 24.5 percent and decreased D_{200} by 49.72 percent.

Figs. 9 to 13 and Table 4 indicate that the increase in the stiffness of the short column which has arisen from the increase in the thickness of the short column plates, raised the amount of P_y and D_y but decreased D_{200}. Since there is no distance between the pyramidal end block and the inner surface of the short column, the added pyramidal end block did not affect P_y and D_y. However, when a part of the short column yields, the pyramidal end block and the inner surface of the short column connect together which reduces D_{200} and steepens up the slope of the force-displacement curve. Based on this, by adding the pyramidal end block to the connection, D200 decreased by 17.88, 22.67, 24.8 and 25.1 percent for CBt10, CBt12, CBt15 and CBt18 respectively.

In order to investigate the effect of adding pyramidal end block, the out-of-plane displacement of the short column plates was considered. The short column has two webs and these webs reshape after applying the loads. Fig. 14 represents the direction of the displacement on the right and left sides of the webs, Figs. 15 to 18 demonstrate the amount of this displacement when force reaches to 200 kN, and Fig. 19 shows the displacement contour of the short column for all of the specimens with and without pyramidal

Table 4 P_y, D_y and D_{200} values for different specimens

Specimen	P_y (kN)	D_y (mm)	D_{200} (mm)	Percentage of increment/decrement (Py)	Percentage of increment/decrement (Dy)	Percentage of increment/decrement (D_{200})
CBt10	60	5.62	358	---	---	---
CBt12	76	6.02	322	+26.6%	+7.12%	-10.06%
CBt15	100	6.78	254	+66.7%	+20.64%	-29.05%
CBt18	116	7	180	+93.3%	+24.55%	-49.72%
				Percentage of increment/decrement compared to the specimens without pyramidal end block		
CBt10P	60	5.53	294	0	-1.6%	-17.88%
CBt12P	76	6.02	249	0	0	-22.67%
CBt15P	100	6.78	191	0	0	-24.8%
CBt18P	116	7	134.9	0	0	-25.1%

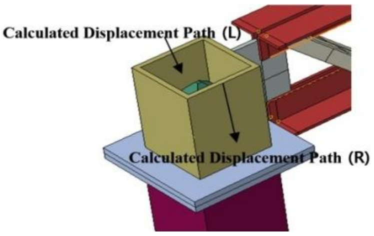

Fig. 14 displacement path in short column webs

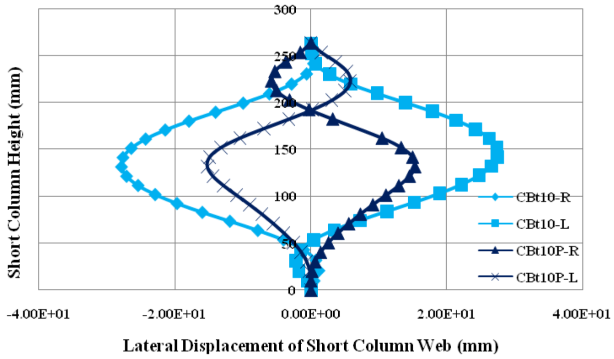

Fig. 15 Out-of-plane displacement curves for CBt10 and CBt10P

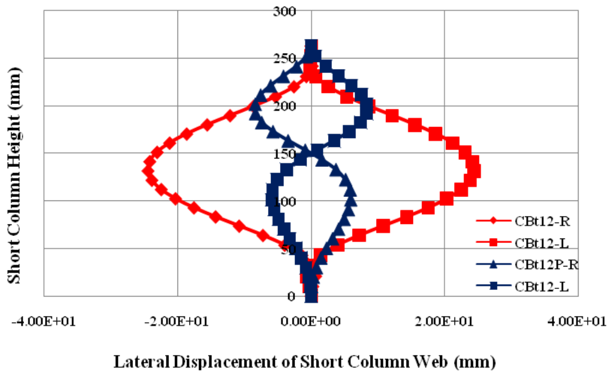

Fig. 16 Out-of-plane displacement curves for CBt12 and CBt12P

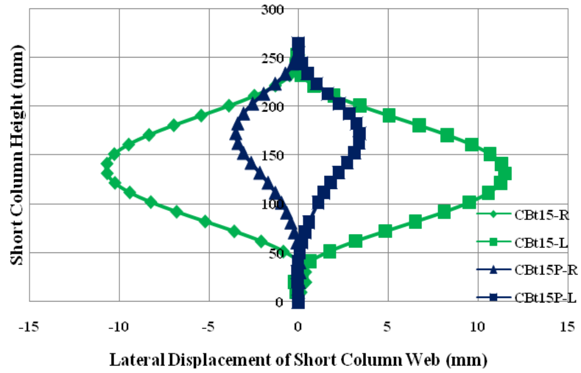

Fig. 17 Out-of-plane displacement curves for CBt15 and CBt15P

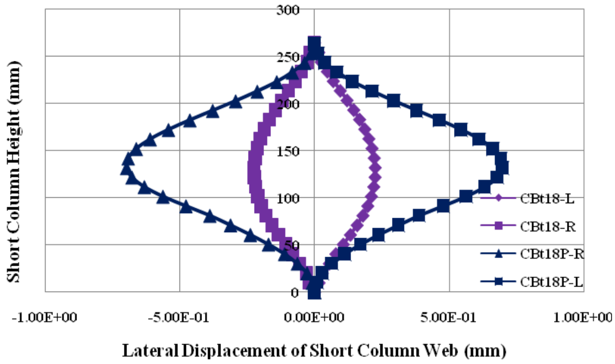

Fig. 18 Out-of-plane displacement curves for CBt18 and CBt18P

end block.

Figs. 15 to 19 indicate that using a pyramidal end block in specimens with smaller short column thicknesses (CBt10, CBt12), the displacement at the bottom of the short column was inwards and at the top of the short column, the displacement was outward. InCBt15, by adding the pyramidal end block, the amount of outward displacement was decreased. In CBt18, when the pyramidal end block

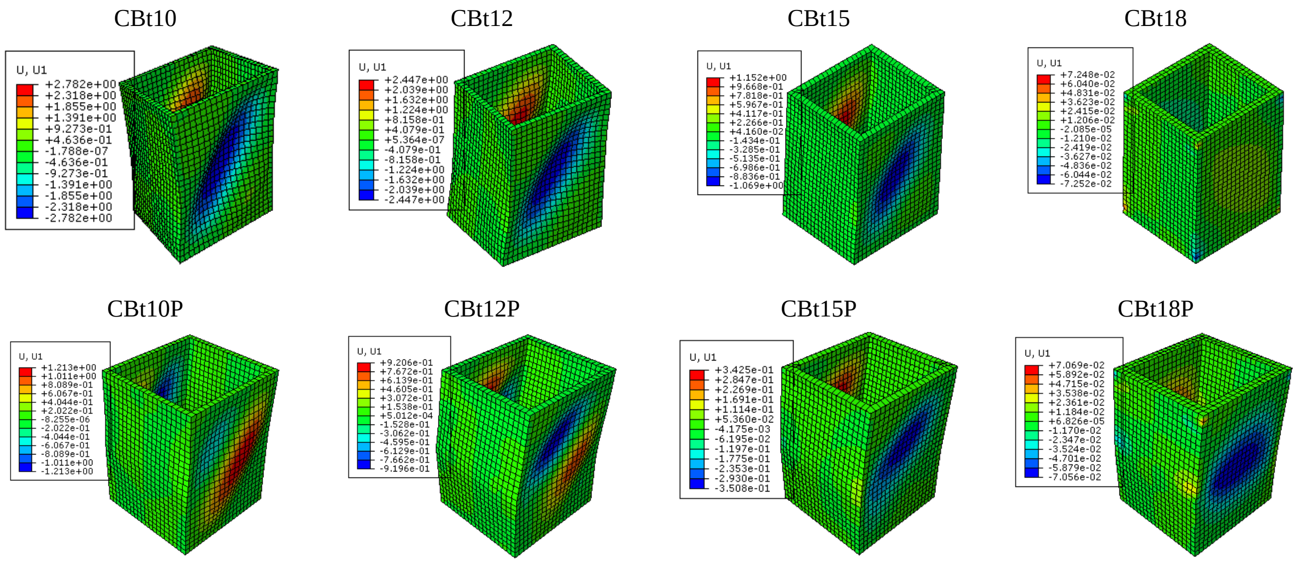

Fig. 19 Out-of-plane displacement contour of short column

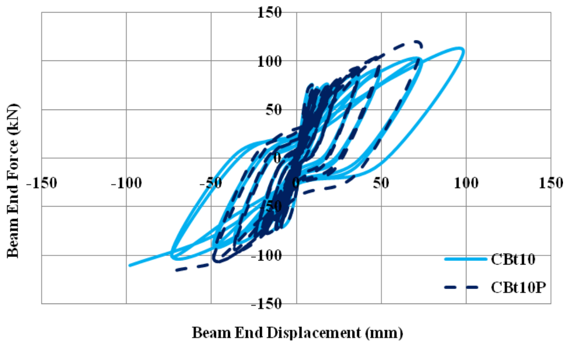

Fig. 20 Force - displacement curve under cyclic loading for CBt10 and CBt10P specimens

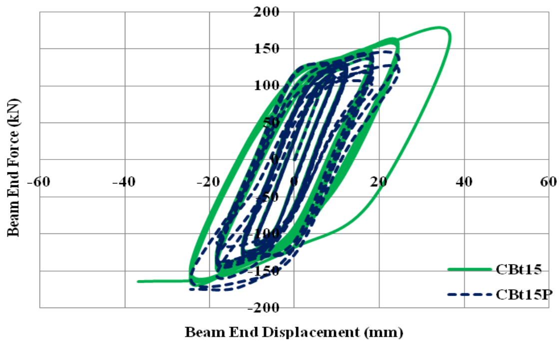

Fig. 22 Force - displacement curve under cyclic loading for CBt15 and CBt15P specimens

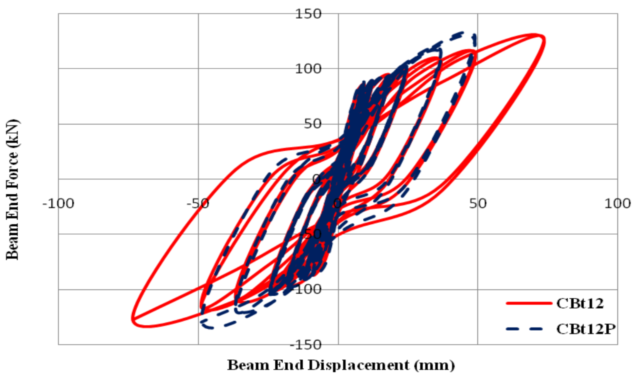

Fig. 21 Force - displacement curve under cyclic loading for CBt12 and CBt12P specimens

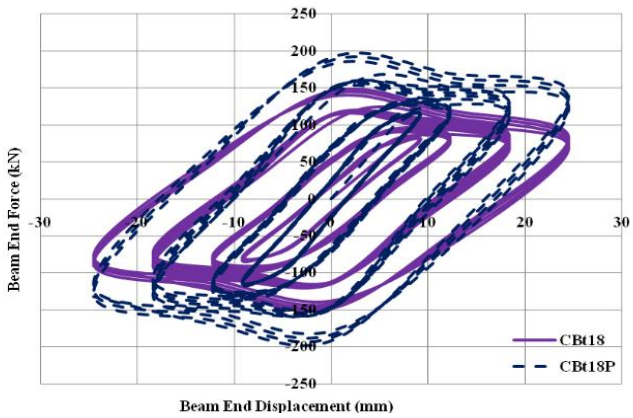

Fig. 23 Force - displacement curve under cyclic loading for CBt18 and CBt18P specimens

was added, the pattern of deformation was changed and the amount of displacement in outward direction increased while the maximum outward displacement of the plate decreased.

Load-displacement curve under cyclic loading is one of the most important curves for any connection. Figs. 20 to 23 show the load-displacement curves for different specimens under SAC2000 loading protocol. In all of the specimens, loading continued until Von Mises stress in one part of the components reached up to the ultimate stress Figs. 20 to 23 show that in specimens with smaller short column thicknesses (CBt10, CBt12), the use of pyramidal end block reduced the connection ductility but increased the amount of bearing capacity for a specific displacement.

In CBt15, by adding the pyramidal end block, the connection ductility and the amount of bearable force for a specific displacement were decreased and in CBt18 and CBt18P, short column failure mode was changed.

Table 5 Summary of numerical specimen details

Specimens	ts (mm)	Bs (mm)	Bp (mm)	Hp (mm)	Pp (mm)	Bc (mm)	tc (mm)	Beam section	Zc (cm^3)	Zb (cm^3)	Zsh.c (cm^3)
S-1-1-1	12	200	172	148	86	200	12	2L80×8.25	636	636	636
S-1.2-1-1[&]	12	200	172	148	86	218	12	2L80×8.25	763	636	636
S-1.4-1-1	12	200	172	148	86	235	12	2L80×8.25	890	636	636
S-1.2-0.9-1	11	198	172	148	86	218	12	2L80×8.25	763	636	573
S-1.2-0.7-1	8.75	193.5	172	148	86	218	12	2L80×8.25	763	636	445
S-1.2-1-0.9	12	200	172	148	86	218	12	2L74×8	763	572	636
S-1.2-1-0.8	12	200	172	148	86	218	12	2L70×7.4	763	509	636
S-1.2-1-0.7	12	200	172	148	86	218	12	2L65×6.85	763	445	636

*S stands for specimens, the first number represents the ratio of column plastic moment to the calculated plastic moment, the second number represents the ratio of short column plastic moment the calculated plastic moment and the third number represents the ratio of beam plastic moment to the calculated plastic moment. Z_c, Z_b and $Z_{sh.c}$ are plastic section modulus for column, beam and short column respectively. Other parameters are shown in Table 3. S-1.2-1-1[&] is the base specimen

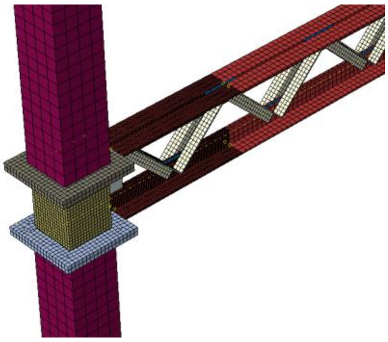

Fig. 24 Finite element model

and properties of the specimens are shown in Table 5. The finite element models were also indicated in Fig. 24.

5.4.1 Force-displacement curve under monotonic loading

In this part, the specimens presented in Table 5 were evaluated under monotonic loading. The plastic moment capacity of the beams was calculated using Eq. (1). The moment value used for the entire connections was 1.15 of the calculated plastic moment. The loading amplitude applied at the end of the beam for all of the specimens began from zero and increased to 72 kN with increment of

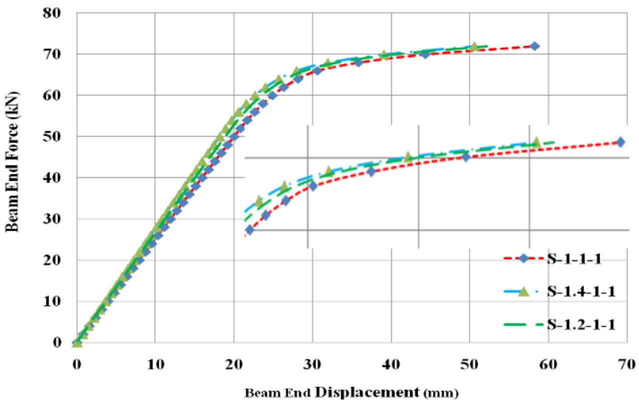

Fig. 25 Force-displacement curves under monotonic loading for specimens with different column plastic moment

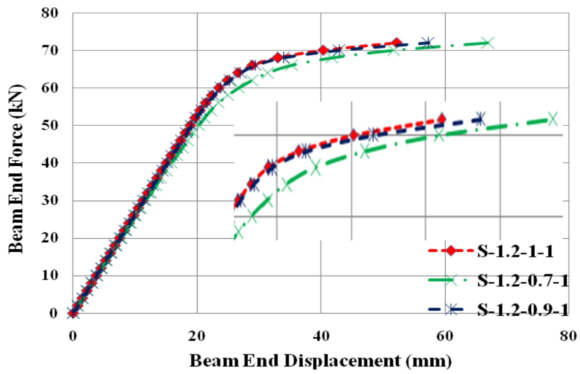

Fig. 26 Force - displacement curves under monotonic loading for specimens with different short column plastic moment

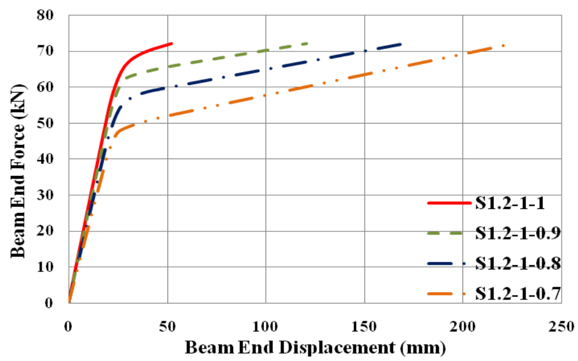

Fig. 27 Force - displacement curves under monotonic loading for specimens with different beam plastic moment

5.4 Effect of different of column, beam and short column sections on connection behavior

In the previous section, the effect of pyramidal end block on connection behavior was evaluated where all components except short column were assumed to be rigid. In this section, in addition to the short column, column, beam and vertical plates are ductile. For this purpose, a specimen with equal amounts of plastic moment (PM_b) for beam and short column and $1.2PM_b$ for column was considered. Then, the effect of these components on the behavior of connection was evaluated by changing the sections of the beam, column and short column. The name

Table 6 P_y, D_y and D_{72} values for different specimens

Specimens	P_y (kN)	D_y (mm)	D_{72} (mm)	Percentage of increment /decrement (P_y)	Percentage of increment /decrement (D_y)	Percentage of increment /decrement (D_{72})
S-1-1-1	53	21.21	58.2	0	+5.68%	+11.54%
S-1.2-1-1*	53	20.07	52.18	-	-	-
S-1.4-1-1	53	19.29	50.59	0	-3.86%	-3.05%
S-1.2-0.9-1	53	20.31	57.36	0	+1.19%	+9.93%
S-1.2-0.7-1	50	20.26	67	-5.66%	+1%	+28.4%
S-1.2-1-0.9	50	19.98	120.54	-5.66%	-0.45%	+131%
S-1.2-1-0.8	43	18.72	170.33	-18.87%	-6.72%	+226.4%
S-1.2-1-0.7	39	18.65	225.2	-26.41%	-7.07%	+331.6%

1 kN. Figs. 25 to 27 represent the force-displacement curves for different specimens. Table 6 demonstrates the amount of P_y, D_y and D_{72} (the amount of beam end displacement when force is 72 kN) for all of the specimens and the changes compared to S-1.2-1-1.

$$PM_b = Z \times F_y = 636*24 \\ = 15264 \text{ kN.cm} = 152.64 \text{ kN.m} \tag{1}$$

Figs. 25 to 27 and Table 6 show that since beam is the first component in connection that yields, the increased stiffness of column does not affect P_y but reduces D_y and D_{72} due to the increase in connection stiffness. Slight decrease of short column stiffness does not affect P_y, D_y and D_{72} but if stiffness decreases substantially, the amount of D_{72} increases because in this case beam and short column yield together. By reducing the section of the beam, connection stiffness as well as P_y and D_y decreases, while D_{72} increases. More specific, a 10 percent reduction in plastic moment reduced P_y and D_y by 5.66 and 0.45 percent respectively and increased D_{72} by 131 percent. A 20 percent reduction in plastic moment also reduced P_y and D_y by 18.87 and 6.72 percent respectively and increased D_{72} by 226.4 percent. In a similar proceeding, a 30 percent reduction in plastic moment reduced P_y and D_y by 26.41 and 7.07 percent respectively while increased D_{72} by 331.6 percent.

5.4.2 Force-displacement curve under cyclic loading

In this part, the specimens presented in Table 5 were evaluated under cyclic loading. Figs. 29 to 36 represent the force-displacement curves for these specimens and Table 7 demonstrates the amounts of displacement and rotation at the yielding (D_y and θ_y) and failure (D_u and θ_u) moment. For the entire specimens, loading continued until the stress values in one part of the components reached to the ultimate stress. Fig. 28, for instance, shows a contour plot of Von Mises stress distribution in the connection components of S-1.2-1-0.9 at the moment when the rotation was 0.04 rad.

Figs. 29 to 36 and Table 7 show that in all of the specimens, beam section yields first and the amount of displacement at the end of the beam at that moment was 24.5 mm (0.01 rad.), except for S-1-1-0.7 for which the displacement was 18.375 mm (0.0075 rad.). In S-1-1-1, S-1.2-1-1 and S-1.4-1-1, plastic hinge formed in beam when the amount of displacement at the end of the beam was 36.75 mm (0.015 rad.) and the force was equal to 68.89, 68.5 and 68.89 kN receptively. In other specimens, no plastic hinge formed in beams. In S-1-1-1, S-1.2-1-1 and S-1.4-1-1, the second section that yields was the web angles of the second row when the displacement at the end of the beam was 49 mm (0.02 rad.), 49 mm (0.02 rad.) and 36.75 mm (0.015 rad.) and the force is 73.32, 65.37 and 60.3 kN respectively. In other specimens, the second section that

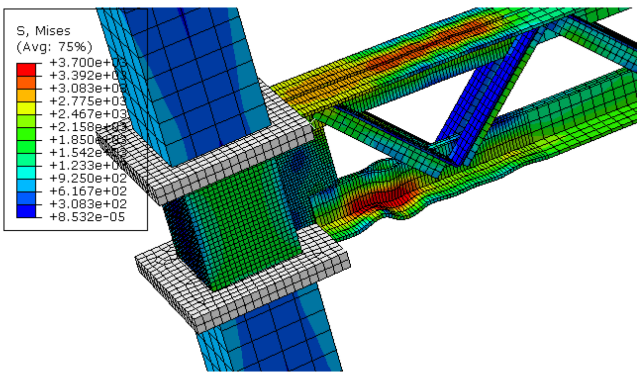

Fig. 28 Von Mises Contour plot of stress distribution in S-1.2-1-0.9

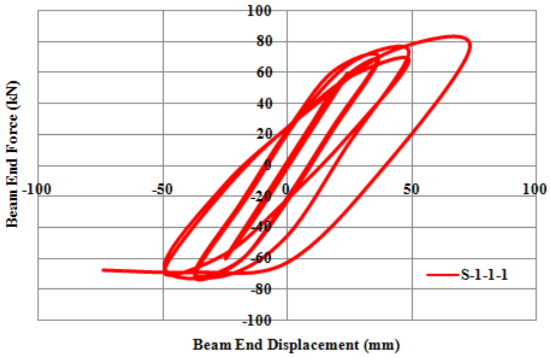

Fig. 29 Force - displacement curve under cyclic loading (S-1.2-1-1).

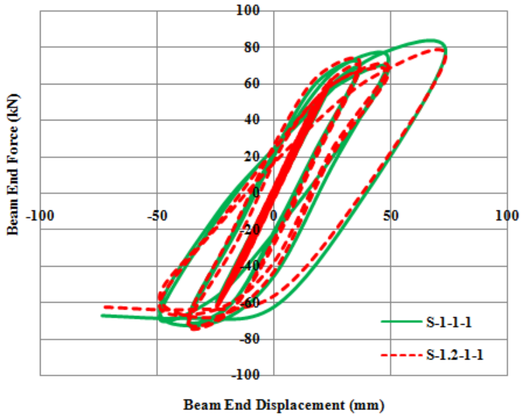

Fig. 30 Force - displacement curve under cyclic loading (S-1.2-1-1 and S-1-1-1).

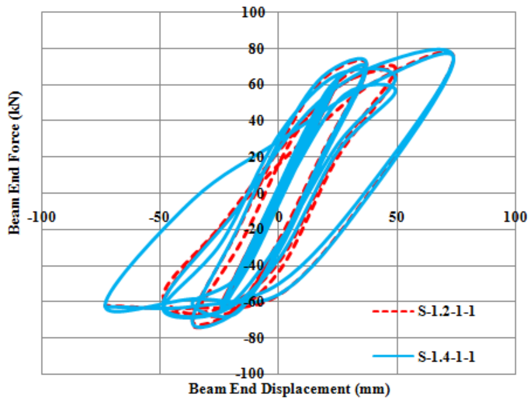

Fig. 31 Force - displacement curve under cyclic loading (S-1.2-1-1 and S-1.4-1-1)

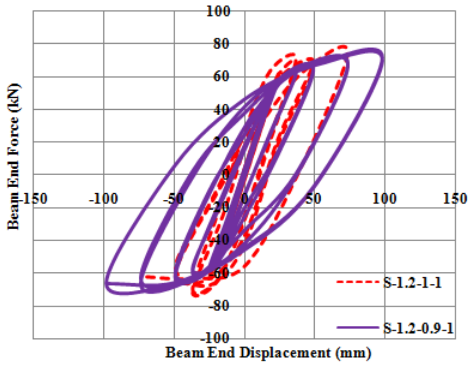

Fig. 32 Force - displacement curve under cyclic loading (S-1.2-1-1 and S-1.2-0.9-1)

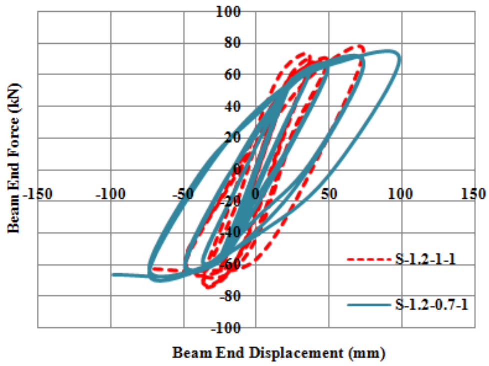

Fig. 33 Force - displacement curve under cyclic loading (S-1.2-1-1 and S-1.2-0.7-1)

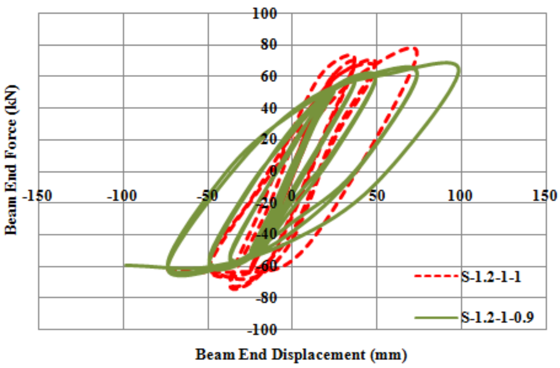

Fig. 34 Force - displacement curve under cyclic loading (S-1.2-1-1 and S-1.2-1-0.9)

yielded was web angles of the first row when the displacement at the end of the beam was 49 mm (0.02 rad.). In S-1-1-0.7, when the displacement at the end of the beam was 24.5 mm (0.01 rad.) and force was 54.86 kN, a part of the short column began to yield.

Popov and Takhirov (2002) suggested that the values of 0.015 and 0.02 radians are the desirable rotation capacity of moment joints. However, the damage caused by Northridge earthquake has cast serious doubt on these limits. On the basis of studies of MRFs, Astaneh-Asl and Nader (1992) proposed a rotational capacity of 0.03 radians. For most specimens, the amount of displacement at the end of the beam at the yielding moment was 24.5 mm (0.01 rad.). For

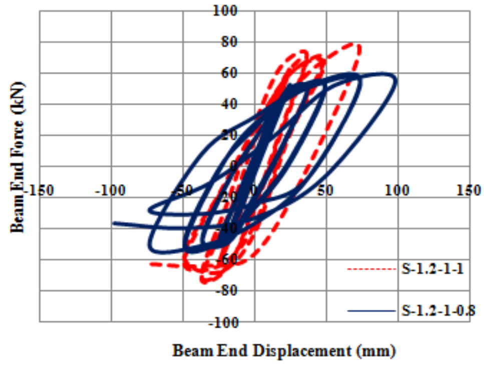

Fig. 35 Force - displacement curve under cyclic loading (S-1-1-1 and S-1-1-0.8)

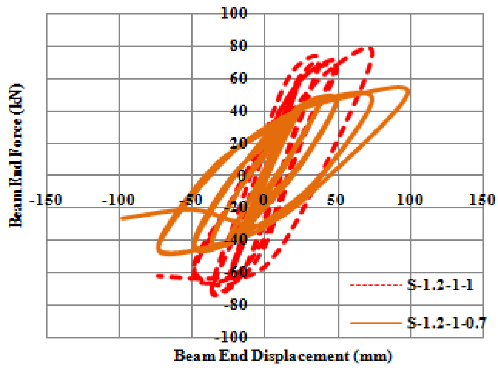

Fig. 36 Force - displacement curve under cyclic loading (S-1-1-1 and S-1-1-0.7)

S-1-1-1, S-1.2-1-1 and S-1.4-1-1, the ultimate displacement was 73.5 mm (0.03 rad.) and for S-1-0.9-1, S-1-0.7-1, S-1-1-0.9, S-1-1-0.8 and S-1-1-0.7 this displacement was 98 mm (0.04 rad.). These amounts imply that by choosing appropriate sections for beam, column and short column, this structural form can develop a good ductility and can be considered as a special moment frame.

5.4.3 Skeleton curve

For a progressive sequence of compressions and tensions, the line joining the peak points in the load–displacement curve of each loading sequence is termed the skeleton curve. In many cases, the skeleton curve coincides with the monotonic loading curve (Elnashai *et al.* 1998).

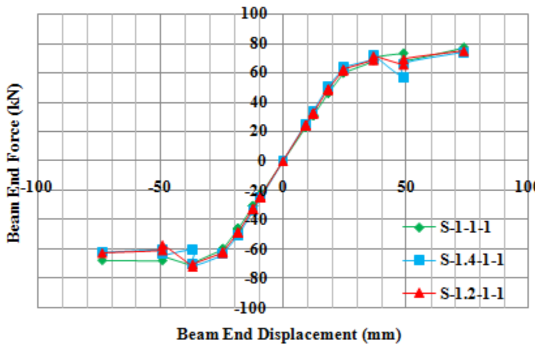

Fig. 37 Skeleton curves for specimens with different column plastic moment

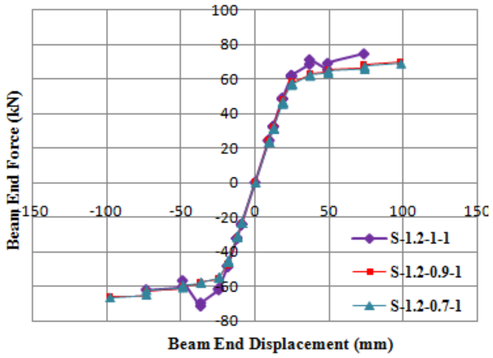

Fig. 38 Skeleton curves for specimens with different short column plastic moment

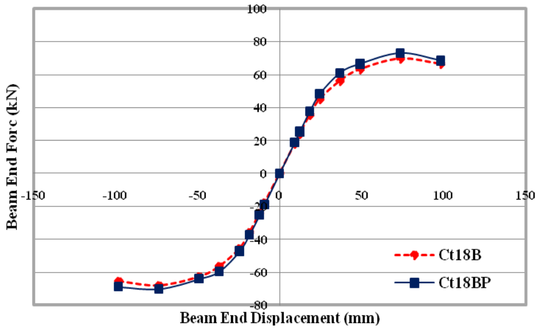

Fig. 41 Skeleton curve of connection with ductile components with and without pyramidal end block

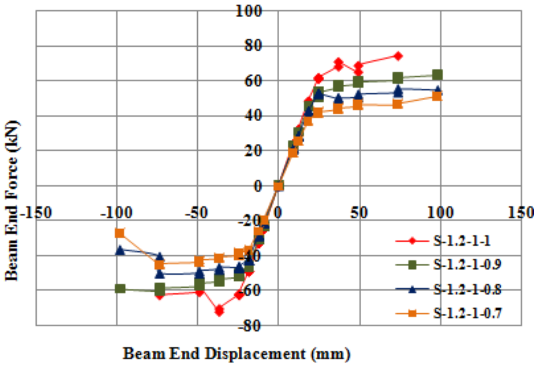

Fig. 39 Skeleton curves for specimens with different beam plastic moment

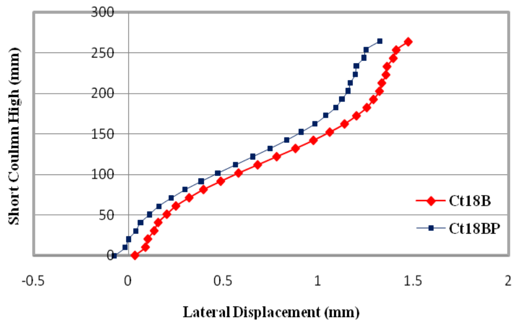

Fig. 42 Lateral displacement curve of sort column with ductile components with and without pyramidal end block

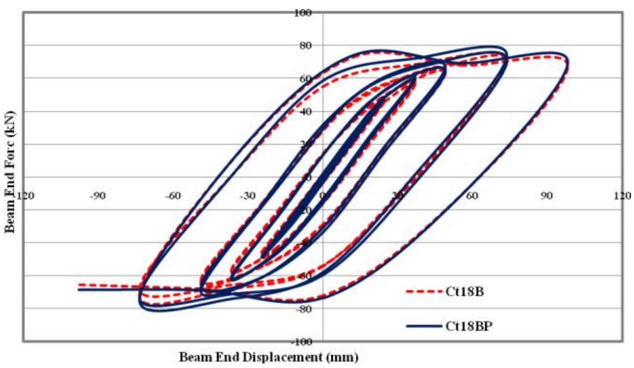

Fig. 40 Force - displacement curve of connection with ductile components with and without pyramidal end block

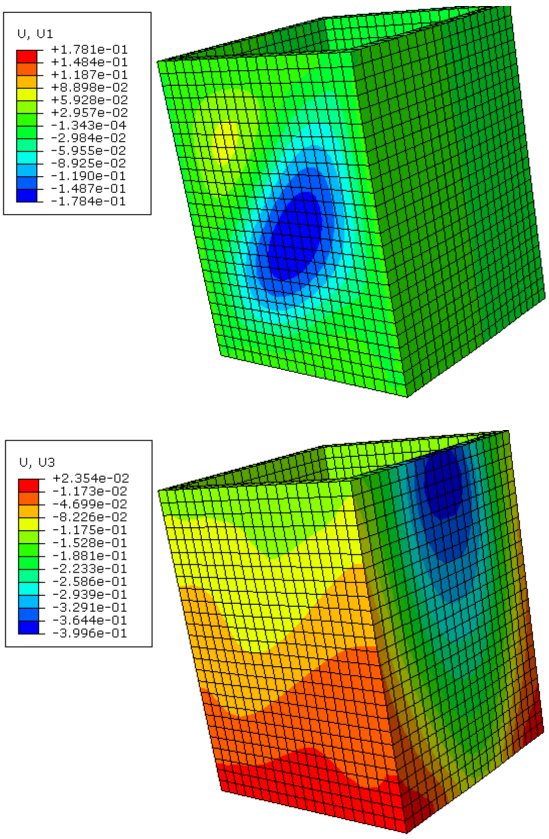

Fig. 43 Displacement contour of short column for U1 and U3 with pyramidal end block

Figs. 37 to 39 compare the skeleton curves of the different specimens. The skeleton curves for the load–displacement well represented the characteristic behavior of the each specimen

Figs. 37 to 39 indicate that the increase in stiffness of the column has negligible effects on the connection behavior. On the contrary, the increase in stiffness of the beam and short column significant affects the ductility of the connection.

5.4.4 Effect of ductility

In this section, the connection was modeled with and

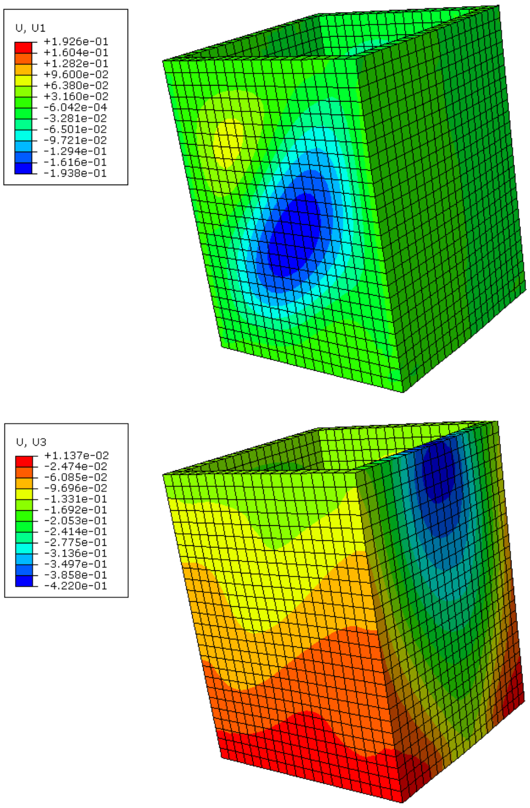

Fig. 43 Displacement contour of short column for U1 and U3 with pyramidal end block

without pyramidal end block in which all the components were ductile. Figs. 40 and 41 show the load-displacement and skeleton curve of the connection with two different configurations (with and without pyramidal end block) under cyclic loading. The curve and the contour of lateral displacement for the short column and the beam end where the loading was applied was represented in Figs. 42 to 44 respectively. In these figures, the two mentioned configurations were once more considered. Since the pyramidal end block behaves like a support inside the short column, it can be seen that using this component not only eases the assembly procedure but also increases the ductility ratio and ultimate load bearing capacity of the connection up to 2 and 3 percent and decreases the lateral displacement of the short column over 10 percent.

6. Conclusions

In this paper, the connection behavior of modular pre-fabricant steel forms was evaluated under monotonic and cyclic loadings and a new geometry was proposed for pyramidal end block. In this way, an experimental specimen was modeled using ABAQUS and the results were compared with the existing experimental data. The research was then continued through changing the main parameters of the connection. The overall results of this study can be summarized as follows:

- The increase in the thicknesses of short column plates increases the stiffness of connection which expands the yielding capacity (Py) and its corresponding displacement of the components (Dy) as well as reducing the beam end displacement under 200 kN (D_{200}).
- Adding a pyramidal end block to the connection facilitates the column assembly particularly in upper stories and, since it acts as a support, it decreases D_{200} and the out-of-plane displacement.
- Due to the distance between the pyramidal end block and inner surface of the short column, using pyramidal end block does not affect P_y and D_y. However, in some specimens, it reduces the ductility and increases the bearing capacity of the connection.
- The increase in the column plastic moment capacity has no significant effect of P_y but reduces D_y and D_{72} consequently. However, due to the decrease in the short column plastic moment capacity, the stiffness of the connection reduces which leads to an increase in D_y and D_{72}. In addition, when the reduction ratio of short column plastic moment capacity is high, the beam and short column yield together and reduces D_y and increases D_{72} consequently.
- The decrease in the beam plastic moment capacity lowers Py and D_y and increases D_{72} consequently. As a result, decreasing the beam plastic moment capacity causes a great portion of the beam displacement to move towards the non-linear region and highly increases D_{72}.
- The entire specimens can bear 0.01 radians within the linear region and 0.04 radians without any reduction in the bearing capacity of the connection. It was also observed that this structural form has a good ductility and can be considered as a special moment frame on condition that the beam, column, and short column are designed to provide higher plastic moment capacity.

References

Akgőnen, A., Yorgun, C. and Vatansever, C. (2015), "Cyclic behavior of extended end-plate connections with European steel shapes", *Steel Compos. Struct., Int. J.*, **19**(5), 1185-1201.

Alhendi, H. and Celikag, M. (2015), "Parametric study on moment–rotation characteristics of reverse channel connections to tubular columns", *J. Constr. Steel Res.*, **104**, 261-273.

Astaneh-Asl, A. and Nader, M.N. (1992), "Cyclic behavior of frames with semi rigid connections", In: *Connections in Steel Structures II: Behavior, Strength, and Design*, Elsevier, Amsterdam, Netherlands, pp. 327-334.

Ataollahi, S., Banan, M. and Banan, M. (2016), "Numerical cyclic behavior of T-RBS: A new steel moment connection", *Steel Compos. Struct., Int. J.*, **21**(6), 1251-1264.

Costa-Neves, L.F., Figueiredo, J.P., da S. Vellasco, P.C.G. and da Cruz Vianna, J. (2013), "Perforated shear connectors on composite girders under monotonic loading: An experimental approach", *Eng. Struct.*, **56**, 721-737.

Elnashai, A.S., Elghazouli, A.Y. and Denesh-Ashtiani, F.A. (1998), "Response of semi rigid steel frames to cyclic and earthquake loads", *J. Struct. Eng.*, **124**(8), 857-867.

FEMA (2000), Recommended seismic design criteria for new steel moment frame buildings, Report no. FEMA-350; Federal Emergency Management Agency: California Universities for

Research in Earthquake Engineering.

Gerami, M., Saberi, H., Saberi, V. and Saedi Daryan, A. (2010), "Cyclic behavior of bolted connections with different arrangement of bolts", *J. Constr. Steel Res.*, **67**, 690-705.

Herrera, R., Bravo, M., Gomez, G. and Aedo, G. (2013), "Performance of built-up T-stubs for Double T moment connections", *J. Constr. Steel Res.*, **88**, 289-295.

Ismail, R.E.S., Fahmy, A.S., Khalifa, A.M. and Mohamed, Y.M. (2016), "Numerical Study on Ultimate Behaviour of Bolted End-Plate Steel Connections", *Latin Am. J. Solids Struct.*, **13**(1), 1-22.

JGJ82-2011 (2011), Technical Specification for High Strength Bolt Connections of Steel Structure; China Building Industry Press, Beijing, China. [In Chinese]

Kulkarni Swati, A. and Gaurang, V. (2014), "Study of steel moment connection with and without reduced beam section", *Case Studies Struct. Eng.*, **1**, 26-31.

Liu, X.C., Pu, S.H., Zhang, A.L., Xu, A.X., Ni, Z., Sun, Y. and Ma, L., (2015), "Static and seismic experiment for bolted-welded joint in modularized prefabricated steel structure", *J. Constr. Steel Res.*, **115**, 417-433.

Maggi, Y.I., Gonçalves, R.M., Leon, R.T. and Ribeiro, L.F.L. (2005), "Parametric analysis of steel bolted endplate connections using finite element modeling", *J. Constr. Steel Res.*, **61**(5), 689-708.

Miller, D.K. (1998), "Lessons learned from the Northridge earthquake", *J. Eng. Struct.*, **20**, 249-260.

Popov, E.P. and Takhirov, S.M. (2002), "Bolted large seismic steel beam-to-column connections part 1: experimental study", *Eng. Struct.*, **24**, 1523-1534.

Sabbagh, A.B., Petkovski, M., Pilakoutas, K. and Mirghaderi, R. (2013), "Cyclic behavior of bolted cold-formed steel moment connections: FE modelling including slip", *J. Constr. Steel Res.*, **80**, 100-108.

Salmon, C., Johnson, J. and Malhas, F. (2009), *Steel Structures*, Pearson/Prentice Hall, Upper Saddle River, NJ, USA.

Smail, R.E.S., Fahmy, A.S., Khalifa, A.M. and Mohamed, Y.M. (2016), "Numerical study on ultimate behaviour of bolted end-plate steel connections", *Latin Am. J. Solids Struct.*, **13**, 1-22.

Zahmatkesh, F., Osman, M.H., Tahir, M.M., Talebi, E. and Kueh, A. (2016), "Numerical study on the structural performance of steel beams with slant end-plate connections", *Latin Am. J. Solids Struct.*, **13**, 1360-1387.

CC